NANO LETTERS
Cite This: Nano Lett. 2018, 18, 2835−2843
Letter
pubs.acs.org/NanoLett

Magnetic Field Sensing by Exploiting Giant Nonstrain-Mediated Magnetodielectric Response in Epitaxial Composites

Min Gyu Kang,*[,†] Han Byul Kang,[†] Michael Clavel,[‡] Deepam Maurya,[†] Sreenivasulu Gollapudi,[†] Mantu Hudait,[‡] Mohan Sanghadasa,[§] and Shashank Priya*[,†]

[†]Bio-inspired Materials and Devices Laboratory (BMDL), Center for Energy Harvesting Materials and Systems (CEHMS), Virginia Tech, Blacksburg, Virginia 24061, United States

[‡]Advanced Devices & Sustainable Energy Laboratory, Virginia Tech, Blacksburg, Virginia 24061, United States

[§]U.S. Army Aviation and Missile Research, Development and Engineering Center, Redstone Arsenal, Alabama 35898, United States

Supporting Information

ABSTRACT: Heteroepitaxial magnetoelectric (ME) composites are promising for the development of a new generation of multifunctional devices, such as sensors, tunable electronics, and energy harvesters. However, challenge remains in realizing practical epitaxial composite materials, mainly due to the interfacial lattice misfit strain between magnetostrictive and piezoelectric phases and strong substrate clamping that reduces the strain-mediated ME coupling. Here, we demonstrate a nonstrain-mediated ME coupling in $PbZr_{0.52}Ti_{0.48}O_3$ (PZT)/$La_{0.67}Sr_{0.33}MnO_3$ (LSMO) heteroepitaxial composites that resolves these challenges, thereby, providing a giant magnetodielectric (MD) response of ∼27% at 310 K. The factors driving the magnitude of the MD response were found to be the magnetoresistance-coupled dielectric dispersion and piezoelectric strain-mediated modulation of magnetic moment. Building upon this giant MD response, we demonstrate a magnetic field sensor architecture exhibiting a high sensitivity of 54.7 pF/T and desirable linearity with respect to the applied external magnetic field. The demonstrated technique provides a new mechanism for detecting magnetic fields based upon the MD effect.

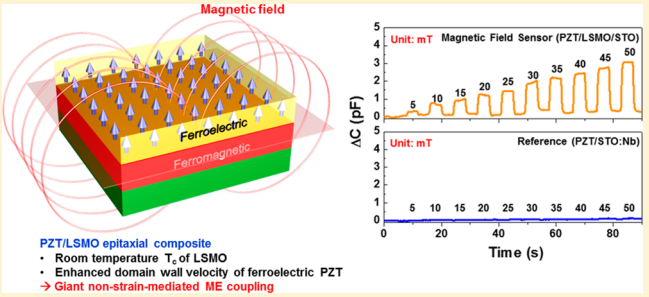

KEYWORDS: *Magnetoelectric, magnetodielectric, epitaxy, PZT, LSMO, magnetic field, sensor*

The magnetoelectric (ME) effect implies coupling between electric polarization and magnetic field (direct effect) or magnetization and electric field (converse effect). This phenomena has attracted significant attention due to its potential applications in tunable devices,[1−3] energy harvesting,[4−11] sensors,[12,13] microwave devices,[14,15] and memory.[16−18] However, none of the currently known single-phase materials have a high enough ME coupling at room temperature (RT) to meet the practical requirements for these applications.[19−21] Composites based on product properties have been shown to overcome the limitations of single-phase materials. ME composites composed of (anti)ferromagnetic and ferroelectric materials, coupled through heterointerfaces, have been found to exhibit strong ME coupling via strain-mediated coupling between the magnetostrictive effect of ferromagnetic materials and the piezoelectric effect of ferroelectric materials.[22] The variation in the direct ME coupling coefficient of composites has been shown to follow the trend in the piezomagnetic coefficient of the ferromagnetic layer.

Recently, 2−2-type heteroepitaxial ME composite thin films have been extensively investigated due to their high ferroelectric and ferromagnetic properties, low leakage current, high quality interface between the ferroic phases, and control of the crystallographic orientation of each layer.[23−27] The strain-mediated direct ME coupling, implying magnetic field-induced piezoelectric potential, has been observed in various heteroepitaxial composites, including ferromagnetic $La_{1-x}Sr_xMnO_3$ and ferroelectric oxides.[23,28,29] However, the lattice misfit strain along with the strong clamping effect from the substrate degrades both piezomagnetic and piezoelectric coefficients resulting in reduced strain-mediated ME coupling. Similarly, the strain-mediated converse ME effect, electric field-induced magnetic moment change, has been negligible in thin epitaxial ME composites, and interface charge-mediated ME coupling has mainly contributed toward modulating the magnetic moment of the ferromagnetic layer.[30−37] On the other hand, avoiding the substrate clamping effect between ferroic phases significantly enhanced the strain-mediated converse ME coupling in epitaxial ferromagnetic films grown on ferroelectric single-crystalline substrates.[38−43] Therefore, relaxation of the substrate clamping effect or development of nonstrain-

Received: December 14, 2017
Revised: February 27, 2018
Published: April 3, 2018

DOI: 10.1021/acs.nanolett.7b05248
Nano Lett. 2018, 18, 2835−2843

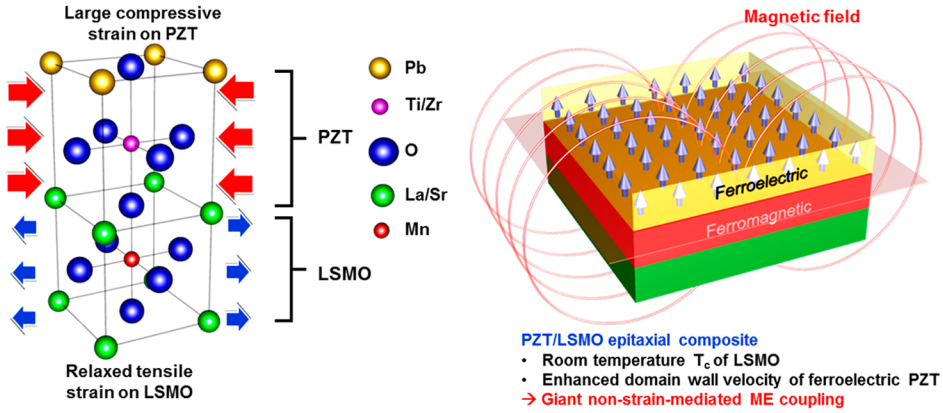

Figure 1. PZT/LSMO heteroepitaxial ME composite. Schematic illustration of (a) PZT/LSMO epitaxial composite film. (b) Giant nonstrain-mediated ME coupling in epitaxial ME composite.

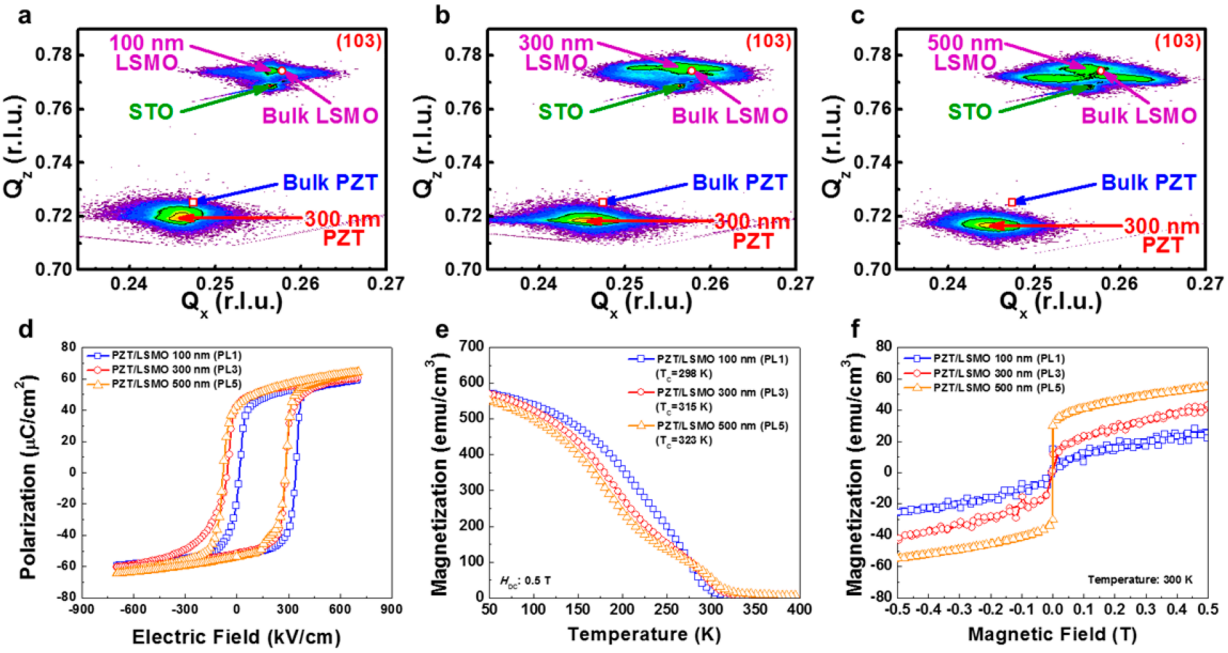

Figure 2. Structural and multiferroic characteristics of the PZT/LSMO heteroepitaxial ME composites. (a) RSM of PZT/LSMO 100 nm (PL1). (b) RSM of PZT/LSMO 300 nm (PL3). (c) RSM of PZT/LSMO 500 nm (PL5). (d) *P-E* curves of PZT/LSMO films with different LSMO thicknesses. (e) Temperature dependence of the magnetization of PZT/LSMO epitaxial films with different LSMO thicknesses. The magnetization values were obtained under an external DC magnetic field of 0.5 T. (f) Room temperature *M-H* curves of PZT/LSMO epitaxial films with different LSMO thicknesses.

mediated coupling dynamics are required for further improvement of the ME response of heteroepitaxial composites.

Magnetodielectric (MD) response is a category of ME coupling effect, which occurs through modulation of the capacitance by external magnetic field. However, expectedly, the magnitude of strain-mediated MD response in multilayer thin film ME systems has been very small, due to the low magnetostriction in thin films as a result of the clamping effect.[28] In this study, we demonstrate a giant MD response in heteroepitaxial ME composites, consisting of ferromagnetic $La_{0.67}Sr_{0.33}MnO_3$ (LSMO) and ferroelectric $PbZr_{0.52}Ti_{0.48}O_3$ (PZT) layers. The giant MD response is attributed to magnetoresistive tuning of domain mobility in PZT that further influences the dielectric dispersion behavior (direct ME effect) and enhanced ferromagnetic properties of the LSMO layer through strain-mediated converse ME effect. The presence of both of these effects simultaneously in the same film allowed the emergence of a giant MD response. Building upon this finding, a magnetic field sensor was realized that exploits the linear change in capacitance with the external magnetic field. The sensor was found to exhibit a high sensitivity, linearity, and stability over a wide range of magnetic field. These results provide a new direction toward advancing ME composites into sensing applications.

Engineering of the lattice strain in *c*-axis oriented epitaxial LSMO and PZT thin films was accomplished by controlling the lattice misfit between the LSMO and PZT layers, as illustrated in Figure 1a. The pseudocubic LSMO exhibits a smaller *a*-axis spacing (3.876 Å)[44] compared to the STO (3.905 Å)[45] substrate, whereas tetragonal PZT (4.044 Å)[46] has a significantly larger lattice parameter, giving rise to the tensile and compressive strains in the LSMO and PZT layers, respectively. The tensile-strained LSMO layer is relaxed with an increasing film thickness, resulting in a large compressive

DOI: 10.1021/acs.nanolett.7b05248
Nano Lett. 2018, 18, 2835−2843

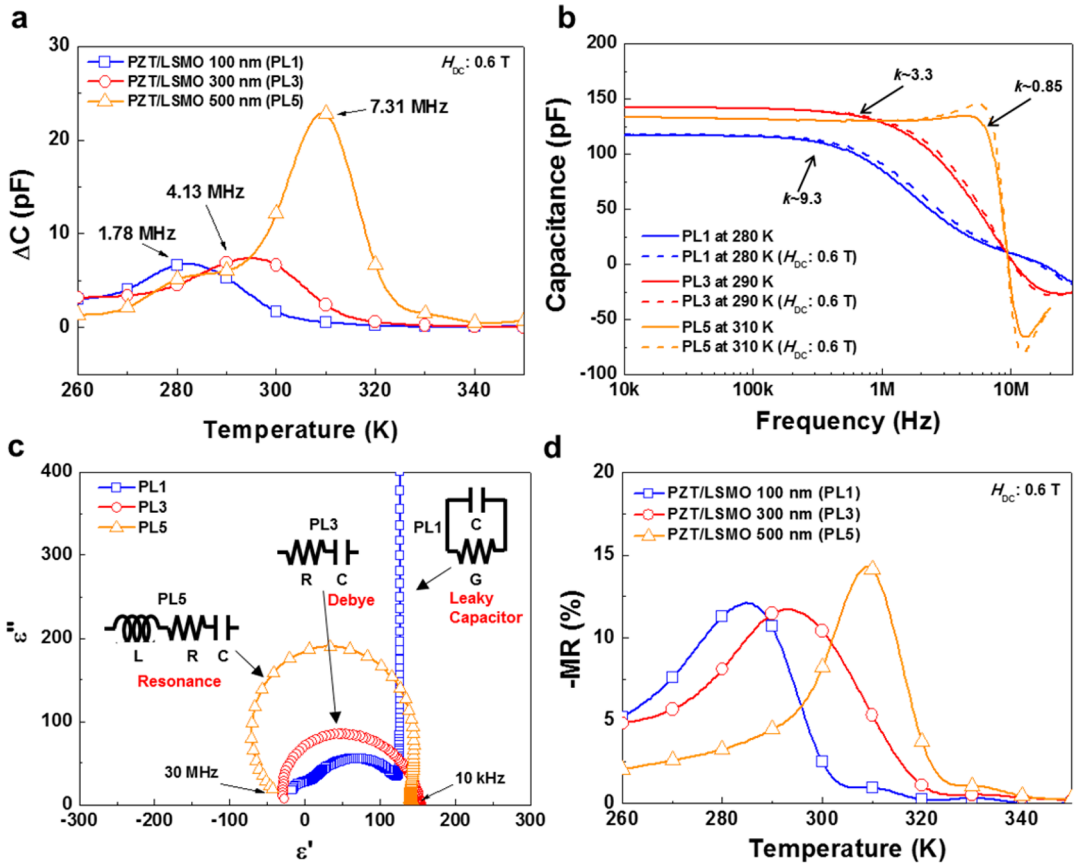

Figure 3. Magnetodielectric characteristics of the PZT/LSMO epitaxial composites. (a) Temperature-dependent MD responses at 1.78, 4.13, and 7.31 MHz for PL1, PL3, and PL5, respectively. Each ME composite exhibited a maximum MD response at these frequencies. (b) Frequency-dependent capacitance spectra of the ME composites (bold lines) and corresponding k constant. The dielectric dispersion behaviors were changed under a 0.6 T magnetic field (dotted lines). (c) Complex dielectric constant spectra and equivalent circuits of the ME composites. (d) Magnetoresistance (MR) response of the ME composites with different measurement temperatures.

strain in the PZT layer that consequently enhances the ferroelectric domain mobility.[47] Furthermore, the relaxed tensile strain in the LSMO shifts the T_C of ferromagnetic phase toward RT. Utilizing this layered architecture, we demonstrate a giant nonstrain-mediated MD response in epitaxial PZT/LSMO composites (Figure 1b).

Different LSMO thickness (100, 300, and 500 nm) p-type conductive ferromagnetic thin films were deposited on Ti-terminated (100) STO substrates, followed by deposition of a 300 nm thick ferroelectric PZT film. These samples will hence be referred to as PL1, PL3, and PL5, respectively. Figure S1a,b show the surface morphology of a Ti-terminated (100)STO substrate and heteroepitaxial PZT/LSMO (500 nm) thin film composite, respectively. The surface morphology of the STO substrate was found to have a terraced structure with one unit-cell-height steps, which assisted in the synthesis of high quality epitaxial thin films. The heteroepitaxial PZT/LSMO thin films also showed step-like structures, indicating that the films were grown through a layer-by-layer epitaxial growth mechanism. Figure S2 shows the X-ray rocking curves for the epitaxial PZT/LSMO thin film composites. The presence of (00l) diffraction peaks indicates the c-axis orientation in the epitaxial growth (Figure S2a,c,e). In order to confirm the strain and lattice relaxation in PZT and LSMO films, an asymmetric reciprocal space map (RSM) analysis was performed around the (103) reflection (Figure 2a–c). The LSMO layers were found to be tensile-strained with respect to STO, whereas the PZT layers were found to be under compressive strain. The c-axis lattice parameter of the LSMO layer is decreased with an increasing thickness of the film ($c_{LSMO,PL1}$ = 3.8703 Å > $c_{LSMO,PL3}$ = 3.8698 Å > $c_{LSMO,PL5}$ = 3.8666 Å), indicating an increased degree of the tensile strain in the thick LSMO layer. However, the large portion of the thick LSMO films (PL3 and PL5) is relaxed as shown in Figure 2a–c. The satellite centroid in the RSM of the PL5 implies a large lattice relaxation through the LSMO films. Because of the large lattice relaxation in the LSMO layer, the reciprocal lattice point (RLP) of the PZT layer shifted toward lower Q_z values with increasing LSMO layer thickness. This indicates a decrease of in-plane lattice parameter in the LSMO, leading to an increase of the residual compressive strain in the PZT layer. Because of the significant residual strain with respect to the LSMO layer, the PZT layers exhibited partially relaxed RLP positions. These relations were confirmed with a high resolution rocking curve analysis, as shown in Figure S2b,d,f. The PL5 sample was found to have the highest compressive strain ($\Delta\omega_{PL1}$: 0.3226° < $\Delta\omega_{PL3}$: 0.3473° < $\Delta\omega_{PL5}$: 0.4113°) and the largest lattice relaxation (fwhm$_{PL1}$ 223″ < fwhm$_{PL3}$ 283″ < fwhm$_{PL5}$ 688″) due to the significant level of compressive strain present within the film.

The ferroelectric behavior of the composites was found to exhibit typical square-shaped hysteresis loops with small leakage currents (Figure 2d). The remnant polarization (P_r) of the films was found to be ~60 μC/cm^2, which is higher than the expected ~50 μC/cm^2.[48] The value of P_r was found to increase

DOI: 10.1021/acs.nanolett.7b05248
Nano Lett. 2018, 18, 2835–2843

slightly with an increasing LSMO layer thickness. The enhanced spontaneous polarization can be attributed to the enhanced tetragonality of the PZT,[49] which is in line with our structural analysis. The *P-E* loops exhibited an asymmetric coercive field (E_c) value due to the imprint effect. (Please see the Supporting Information.) Moreover, the composites were found to have a similar piezoelectric response due to the clamping effect induced by the substrate (Figure S3).

In order to evaluate the ferromagnetic characteristics of the LSMO layers, magnetization measurements were performed as a function of temperature and DC magnetic field (Figure 2e,f). The Curie temperature (T_c) was shifted toward lower temperatures in the 100 nm thick LSMO film (~298 K), which corresponds to the case of the highest tensile strain with respect to the STO substrate. Conversely, the 500 nm thick LSMO film exhibited a higher T_c (~323 K) resulting from relaxed tensile strain, which is in agreement with prior reports.[50] The LSMO films were found to exhibit soft ferromagnetic behavior with low coercive fields ($H_c \sim 0.34$ μT). The 100 nm thick LSMO film had a T_c near RT and small magnetization (~25 emu/cm^3 under 0.5 T). However, the 500 nm thick LSMO film exhibited substantial magnetization (~54 emu/cm^3 under 0.5 T) as shown in Figure 2f. This is expected as the volumetric density of magnetic domains increases and substrate clamping decreases with the increasing thickness.

The MD response, magnetic field-induced dielectric tunability, in the epitaxial PZT layers was evaluated as a function of frequency (10 kHz-30 MHz) at various temperatures from 260 to 350 K (Figure 3). The variation of capacitance (MD coefficient) can be expressed as

$$\text{MD}\ (\%) = \frac{\Delta C}{C_0} \times 100 \tag{1}$$

where ΔC and C_0 are the capacitance change and the capacitance at zero magnetic field, respectively. The MD response of the PZT/LSMO composites were found to vary with temperature and frequency as shown in Figure 3a. The MD response maximized at a certain frequency in the dielectric relaxation region (Figures S4−S7), and the frequency presenting the maximum MD response increased with an increasing thickness of the LSMO layer (Figure S4). The highest MD response was observed near T_c of the LSMO layer, and the MD coefficient of the PZT/LSMO composites was found to increase with an increasing LSMO layer thickness. In particular, PL5 exhibited a capacitance change with a 24% MD coefficient under a 0.6 T DC magnetic field near RT.

Since the strain-mediated MD response in thin film ME composites is weak due to substrate clamping, a major contributing factor for a large MD effect is considered to be the coupling of magnetoresistance (MR) and the Maxwell−Wagner (MW) effect, which shifts the dielectric relaxation frequency of the multiferroic capacitor.[28,51,52] The MW effect in the case of the magnetoresistive materials can be approximated by considering leaky dielectric layers in series. To reveal the origin of the MD behavior in epitaxial ME composites and its temperature and frequency dependence, the dielectric dispersion of the PZT/LSMO composites was investigated using a damped harmonic oscillator model. The frequency dependence of the complex dielectric constant and its relaxation and absorption behavior can be expressed as[53−55]

$$\varepsilon^*(\omega) = \varepsilon_\infty + \frac{\omega_r^2(\varepsilon_s - \varepsilon_\infty)}{\omega_r^2 - \omega^2 + 2j\alpha\omega} \tag{2}$$

where, ε_s, ε_∞, ω, and ω_r are the static dielectric constant, high frequency limit of the dielectric constant, angular frequency, and resonance frequency, respectively, and α is the damping coefficient of the dielectric response, which is responsible for the damping of the dipole motion. Using α, the parameter k, which is a factor for identifying the dielectric dispersion mechanism, can be calculated through the relationship $k = 2\alpha/\omega_r$. When k is smaller than 1 ($k < 1$), resonance-type dielectric dispersion dominates the dielectric behavior. The behavior gradually changes to relaxation-type dielectric dispersion with an increasing k value. From eq 2, the real and imaginary parts of the complex dielectric constant can be derived as

$$\varepsilon'(\omega) = \varepsilon_\infty + \frac{\omega_r^2(\varepsilon_s - \varepsilon_\infty)(\omega_r^2 - \omega^2)}{(\omega_r^2 - \omega^2) + 4\alpha^2\omega^2} \tag{3}$$

$$\varepsilon''(\omega) = \frac{2(\varepsilon_s - \varepsilon_\infty)\alpha\omega_r^2\omega}{(\omega_r^2 - \omega^2)^2 + 4\alpha^2\omega^2} \tag{4}$$

Using eq 3, the dielectric dispersion behavior and corresponding k value were calculated for each PZT/LSMO composite (Figure S8). Figure 3b shows the variation in the frequency-dependent capacitance spectra under a DC magnetic field. The dielectric dispersion behavior was found to significantly change from relaxation-type (PL1 and PL3) to resonance dominated relaxation (PL5) depending upon the LSMO thickness. The calculated k values were 9.3, 3.3, and 0.85 for PL1, PL3, and PL5, respectively. This indicates that the damping coefficient of the PZT layer is significantly influenced by the thickness of the LSMO layer.

The origin of the dielectric dispersion behavior in ferroelectric materials has been attributed to domain wall motion because the main contribution to the dielectric response is directly associated with the ferroelastic and/or ferroelectric polarization.[56−58] In ferroelectric materials, residual strain is one of the factors affecting the domain wall motion. Prior research has shown that the domain wall velocity of (001) oriented epitaxial PZT films tends to increase in proportion to an in-plane biaxial strain.[47] Mechanical strain has been found to reduce the damping coefficient and change the dielectric dispersion behavior from relaxation-type to resonance-type in the bulk ferroelectric ceramic.[56] In addition to strain, the domain wall motion can also be modulated through the resistance (or resistivity) of the electrodes because the domain wall velocity is dependent on the electric current that flows to the domain wall in order to compensate the in-bound polarization charge.[59,60] Figure 3c shows a complex dielectric spectra and the equivalent circuits for the composites. PL5 was found to exhibit a clear resonance oscillation circle, which is attributed to series-connected $L_{eq}-R_{eq}-C_{eq}$ elements in equivalent circuit, where L_{eq}, R_{eq}, and C_{eq} are inductance, resistance, and capacitance in an equivalent circuit, respectively.[55] Because the L_{eq} element is determined by the conductivity of the LSMO and PZT, a low resistance of the thicker LSMO layer in PL5 increases L_{eq}, leading to resonance. In contrast, PL1 exhibited a leaky capacitor-like behavior in the low frequency region, and the PL3 semicircle spectra indicate a fully damped Debye relaxation behavior. Hence, we conclude that the high degree of in-plane strain induced in the PZT layer and relatively low resistance of the thicker LSMO in PL5 could

DOI: 10.1021/acs.nanolett.7b05248
Nano Lett. 2018, 18, 2835−2843

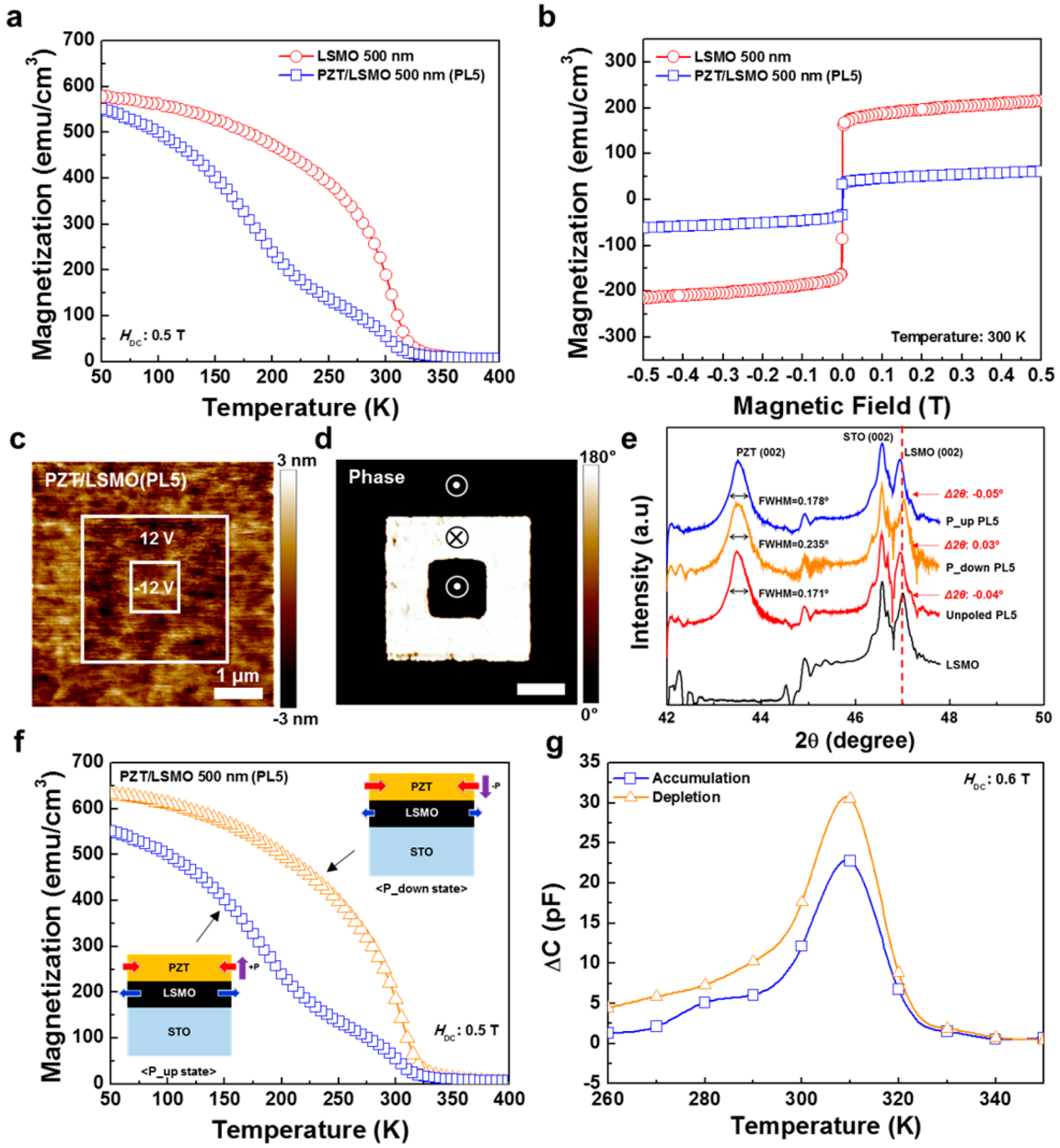

Figure 4. Interface charge modulation for enhancing the MD response (a) Temperature dependence of the magnetization of PL5 and pristine 500 nm thick epitaxial LSMO. (b) Room temperature *M-H* curves of PL5 and pristine 500 nm thick epitaxial LSMO. (c) Surface AFM image of PL5 with a marked polarization switching voltage condition; DC biases of 12 V and −12 V were applied on a 3 × 3 μm^2 area and 1 × 1 μm^2 area. (d) Piezoelectric response phase image. Arrows indicate polarization direction. (e) XRD patterns of pristine LSMO and PL5 depending on poling direction. (f) Temperature dependence of magnetization with a different polarization direction of the PZT layer. (g) Temperature-dependent MD response of PL5 film with a different polarization direction of the PZT layer.

be contributing factors toward reduction of the damping coefficient, which in turn changes the dielectric dispersion behavior to resonance type. This phenomena is more obvious in the temperature-dependent resistance variation of the LSMO layer, which was found to peak at T_c (Figure S9). The LSMO exhibited a metallic behavior below T_c and a semiconductor-like transport behavior above T_c. The temperature-dependent capacitance of the PZT layer at the frequency exhibiting a maximum MD was found to show a similar trend as the resistance change of the LSMO layer, and the dielectric dispersion behavior trended with the resistance variation (Figure S10). This demonstrates that the resistance of the LSMO layer affects the dielectric dispersion behavior of the PZT layer.

Under a 0.6 T DC magnetic field, the dielectric dispersion behavior of the PZT/LSMO composite was transformed toward a resonance dominated-type response having a low damping coefficient (dashed line in Figure 3b). It is known that LSMO has a large MR effect near T_c.[61] Based upon the prior studies describing the relationship between the resistance change of the LSMO layer and the dielectric dispersion behavior of the PZT, we expect that the large MD effect near T_c stems from a large MR effect. To clarify this result, we have measured the DC magnetic field-induced resistance change of

DOI: 10.1021/acs.nanolett.7b05248
Nano Lett. 2018, 18, 2835−2843

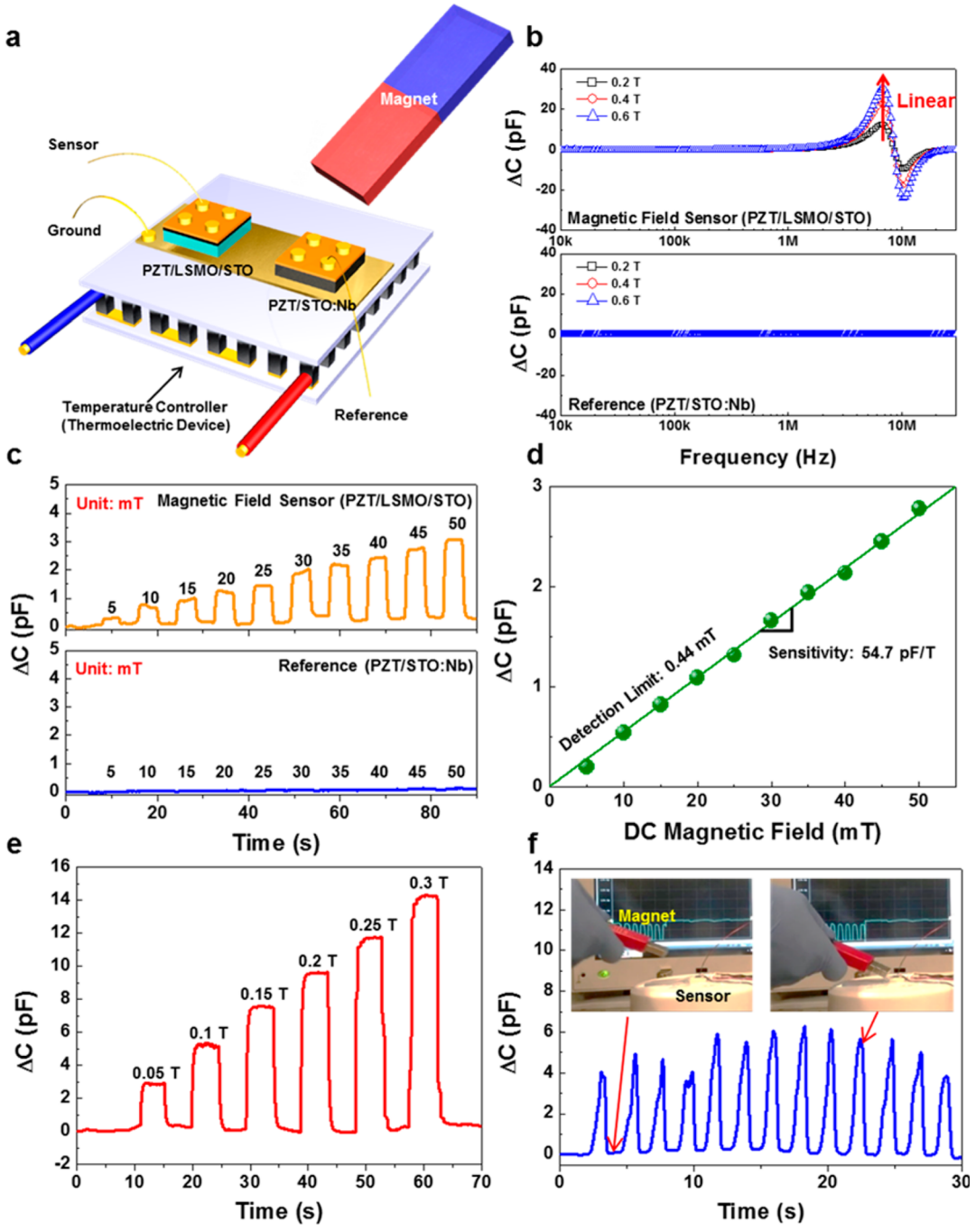

Figure 5. Magnetic field sensor based on MD effect. (a) Schematic illustration of the magnetic field sensor. (b) Frequency-dependent MD response in the sensing and reference elements. (c) DC magnetic field response from sensing and reference elements with various field strengths. A homogeneous pulsed DC magnetic field (5 s pulse width) was applied along the in-plane direction of the sensor. (d) Linear calibration curve from the sensor response signal. (e) DC magnetic field response from sensing and reference elements under a strong field strength. (f) Magnetic field response of the sensor under the dynamic magnetic field change.

the LSMO layer as a function of temperature (Figure 3d). The MR coefficient of LSMO was calculated using the expression

$$\mathrm{MR}\ (\%) = \frac{\Delta R}{R_0} \times 100 \tag{5}$$

where ΔR and R_0 are the resistance change under the magnetic field and the resistance at zero magnetic field, respectively. The MR effect was maximized near T_c of the LSMO layer, exhibiting a similar trend to that of the MD behavior shown in Figure 3a. However, the magnitude of the responses in MR is similar across all samples, while PL5 exhibited a significant MD response compared to other composites in the resonance region. In a prior study, temperature-dependent resistance change in the LSMO layer has been shown to result in a large capacitance tunability in the resonance region (Figures S9 and S10). Therefore, we conclude that the large MD effect in PL5 is attributed to the coupling between the large MR effect in the LSMO and resonance driven dielectric dispersion behavior. This phenomena results from the low dielectric damping

DOI: 10.1021/acs.nanolett.7b05248
Nano Lett. 2018, 18, 2835−2843

coefficient achieved through the large lattice strain in the PZT layer as well as the low resistance of the LSMO electrode.

The magnetic moment of the ferromagnetic layer in the ME composite is a crucial factor for determining the magnitude of the magnetic field-induced coupling effect. To enhance the MD response in the ME composite, we investigated the influence of the ferroelectric polarization direction of the PZT on the magnetic moment of the LSMO layer, which is referred as converse ME effect. Figure 4a,b shows the temperature-dependent magnetization and RT magnetization-DC magnetic field (*M-H*) curve for a 500 nm thick pristine LSMO film grown on an STO substrate and PL5, respectively. The initial magnetic properties of the LSMO films were found to degrade following PZT deposition. In prior reports, it has been shown that the modulation of the magnetic properties in an epitaxial ME composite results from interface charge-mediated converse ME coupling[30−37] and strain-mediated ME coupling across the ferroelectric/ferromagnetic interface.[38−43] In the case of interface charge-mediated converse ME coupling, the interfacial magnetization is changed due to electrostatic charge accumulation at the PZT/LSMO interface from ferroelectric spontaneous polarization.[35,62−64] Prior studies have shown that interfacial charge accumulation modulates the valence state of Mn from the high spin state Mn^{3+} (S = 2) to the low spin state Mn^{4+} (S = 3/2) near the interface. This results in an interfacial ferromagnetic to antiferromagnetic phase transition in the accumulation state and, thereby, changes the magnetic moment of LSMO. However, the interface charge-mediated ME effect is largely responsible for coupling between the ultrathin (<4 nm) LSMO film and PZT layer. As the film thickness increases, the contribution of the strain-mediated converse ME effect is increased toward modulation of the magnetic moment. The driving force provided by strain-mediated converse ME coupling in the epitaxial ME composite is the piezoelectric strain originating from the ferroelectric layer, which causes strain in the ferromagnetic layer across the interface, resulting in modulation of the magnetic anisotropy of the ferromagnetic layer via magnetoelastic coupling. Therefore, the degradation of the magnetic moment in PL5 results from strain-related magnetic modulation.

To investigate the influence of the polarization direction of the PZT layer on a piezoelectric strain in a 500 nm thick LSMO layer, the initial polarization state and ferroelectric domain structure of the PZT film were analyzed by using piezoelectric force microscopy (PFM), as shown in Figure 4c,d. Switching of the ferroelectric polarization was accomplished by poling with a 12 V and −12 V DC bias by scanning the sample surface over 3 × 3 μm^2 and 1 × 1 μm^2 areas, respectively. PL5 was initially found to have a single-phase ferroelectric domain. The data clearly show a 180° domain motion without pinned domain walls, as shown in Figure 4d. The polarization direction was determined from the corresponding poling direction. As a result, the initial polarization exhibited the upward direction (outer region in Figure 4d). To quantify the piezoelectric strain in the PZT/LSMO composite depending upon the polarization direction of the PZT layer, XRD patterns for pristine LSMO, as-deposited PL5, and poled PL5 with a different polarization direction were analyzed as shown in Figure 4e. It was found that the amplitude of tensile strain in the LSMO layer is increased following PZT deposition, compared to the pristine LSMO film, because of the large in-plane lattice parameter of the PZT layer. This indicates that the tensile strain in the LSMO layer arising from the PZT layer results in degradation of the magnetization in the PZT/LSMO epitaxial composite (Figure 4a,b). The polarization direction was switched to a downward direction in the overall PZT film area (P_down state) by the corona poling process, which enables noncontact polarization switching in the overall area (Figure S11a). After polarization switching, the PZT (002) peak was found to broaden, which indicates lattice relaxation due to an excessive induced piezoelectric compressive strain, while the amplitude of the tensile strain in the LSMO layer was relaxed as compared to the pristine LSMO film. The relaxed tensile strain in the LSMO layer results in recovery of the magnetization of the PZT/LSMO composite (Figure 4f). When the polarization direction of the PZT layer was upward (P_up state), tensile strain in the LSMO is again increased similar to the case of the unpoled composite. Therefore, we conclude that a large converse ME effect in the PL5 composite is mainly contributed due to the piezoelectric strain-mediated magnetoelastic coupling (Figure S12). Through recovering the entire magnetic moment in the PZT/LSMO composite, the RT magnetization of PL5 is ∼3.4 times larger in the P_down state (Figure S11b), and the depressed magnetization is nearly recovered as the measurement temperature decreases. Further, the enhanced magnetic properties of the LSMO layer resulted in the improved MD response in PL5 (Figure 4g). The temperature-dependent MD response in the P_down state exhibits a similar trend in the P_up state (Figures 4g and S13); however, the tunable capacitance range was enlarged in the P_down state, wherein the maximum MD coefficient was found to be ∼27% under a DC magnetic field of 0.6 T.

Utilizing the giant MD response in the epitaxial PZT/LSMO composite with the P_down state in PL5, we have demonstrated a highly sensitive DC magnetic field sensor that operates using a novel sensing mechanism, as illustrated in Figure 5a. To maintain an operating temperature at 310 K, a thermoelectric device was mounted under the PZT/LSMO composite as a temperature controller. To fabricate sensing elements, 200 μm diameter circular patterns were formed on the PZT/LSMO composite. The capacitance of the sensing elements was measured between the LSMO layer and the top of the pattern via Cu wire connections. A reference element was prepared to simultaneously detect a non-MD coupled capacitance change, such as inductive noises caused by the surrounding stray electromagnetic field. For the reference element, a 300 nm thick epitaxial PZT thin film was deposited on a conducting and nonmagnetic 0.5 wt % Nb doped STO (STO/Nb) substrate under the same deposition conditions as PL5. The synthesized reference PZT layer showed an excellent ferroelectric behavior (Figure S14). Figure 5b displays the MD response in the sensing and reference elements. The MD response of the sensing element was found to linearly increase with an increasing DC magnetic field strength, whereas the reference element does not exhibit any MD response throughout the investigated frequency range.

To evaluate the sensing performance of the magnetic field sensor, the capacitance change of the sensor was monitored at 7 MHz under a pulsed DC magnetic field applied along the in-plane direction of the sensor (Figure 5c). The sensing element exhibited a dynamic capacitance change that linearly increased with the DC magnetic field, ranging from 5 to 50 mT. In contrast, the reference element does not show any response from the magnetic field. The sensor exhibited a near perfect linearity (Figure 5d). The calculated sensitivity (sensitivity = $\Delta C/\Delta H$, where ΔC and ΔH are the capacitance change and

DOI: 10.1021/acs.nanolett.7b05248
Nano Lett. 2018, 18, 2835−2843

magnetic field change, respectively) of the sensor was found to be ~54.7 pF/T. To evaluate the lowest detectable magnetic field strength, the theoretical detection limit of the MD sensor was extrapolated from the linear calibration curve. Because the sensing signal is considered to be a true signal when the signal-to-noise ratio equals 3, the detection limit can be calculated through relation:[65,66]

$$\text{detection limit} = 3\frac{\text{RMS}_{\text{noise}}}{\text{slope}} \quad (6)$$

From the calculated detection limit, we expect that the MD sensor can detect a magnetic field down to 0.44 mT. Furthermore, the linearity of the sensor was found to exhibit stability under a wide magnetic field range (Figure 5e). This sensor was highly sensitive and exhibited a fast response under a dynamic magnetic field operation (Figure 5f and supporting movie). The sensor exhibited a large capacitance change when the permanent magnet was in close proximity to the sensor (~1 cm), after which the baseline capacitance value was recovered within a short duration (~0.1 s) following the removal of the permanent magnet.

In conclusion, we have achieved a giant MD response near RT in epitaxial ME composites through the direct ME effect (i.e., tuning the polarization dispersion behavior of PZT by the MR effect) and converse ME effect (i.e., tuning the magnetic moment of LSMO by piezoelectric strain-induced magnetoelastic coupling). The origin of the large MD effect in epitaxial composites was revealed by a systematic investigation of magnetic field-induced changes in dielectric behavior through the damped harmonic oscillator model. The resonance-type dielectric dispersion behavior in ME composites, resulting from a high degree of compressive strain applied on the PZT layer and the low resistance of the LSMO layer, was found to enhance the MD response when coupled with the MR effect. The magnetization of the LSMO layer is depressed after PZT deposition due to an increased amplitude of tensile strain. To relax the tensile strain and recover the magnetic properties of LSMO, we demonstrated polarization switching to the P_down state throughout the film using the corona poling technique. Following this procedure, the PZT/LSMO composite exhibited a giant MD response of ~27%. The giant MD response was utilized to fabricate highly sensitive magnetic field sensors, which successfully detected both dynamic and static magnetic fields. The sensitivity and detection limit of the sensor were found to be 54.7 pF/T and 0.44 mT, respectively. We believe that our MD effect-based magnetic sensing technique will open new opportunities in developing miniature on-chip sensors for feedback controls in electronics and various other control applications.

■ ASSOCIATED CONTENT

Supporting Information

The Supporting Information is available free of charge on the ACS Publications website at DOI: 10.1021/acs.nanolett.7b05248.

Experimental method details, structural properties of ME composites, ferroelectric imprint effect in ME composites, piezoelectric response of ME composites, MD characteristics of ME composites, frequency dependence of dielectric spectra of PL1, PL3, and PL5 with various applied magnetic fields and temperatures, calculated frequency-dependent dielectric spectra, temperature dependence of resistance and capacitance in ME composites, frequency-dependent dielectric spectra of epitaxial ME composites at various temperatures, corona poling, strain-mediated converse ME coupling, frequency dependence of dielectric spectra of P_down PL5 with various applied magnetic fields and temperatures, and ferroelectric P-E loop of reference element (PDF)

Video of sensor (ZIP)

■ AUTHOR INFORMATION

Corresponding Authors

*E-mail: mgkang@vt.edu.

*E-mail: spriya@vt.edu.

ORCID

Min Gyu Kang: 0000-0001-9247-6476

Michael Clavel: 0000-0002-2925-6099

Author Contributions

M.G.K. suggested the concept of the study, conducted the experiments, and developed the draft of manuscript. H.-B.K. contributed to preparing the samples and characterization of magnetic properties. M.C. and M.H. performed the X-ray diffraction and XPS studies. D.M., S.G., and M.S. contributed to the discussion of the results. S.P. initiated the study and was responsible for the directions of the overall research. All authors discussed the results and contributed to the writing of the manuscript.

Notes

The authors declare no competing financial interest.

■ ACKNOWLEDGMENTS

M.G.K. and H.B.K. acknowledge support from the Air Force Office of Scientific Research through grant no. FA9550-14-1-0376 (Ali Sayir). D.M. and S.G. were supported through the Department of Energy, Office of Basic Energy Science grant no. DE-FG02-06ER46290. S.P. acknowledges the support from the Office of Naval Research through the NSF I/UCRC: Center for Energy Harvesting Materials and Systems (CEHMS) membership. M.C. acknowledges support from the National Science Foundation under grant no. ECCS-1507950.

■ REFERENCES

(1) Ma, J.; Hu, J. M.; Li, Z.; Nan, C. W. *Adv. Mater.* **2011**, *23*, 1062−1087.

(2) Chu, Y. H.; Martin, L. W.; Holcomb, M. B.; Gajek, M.; Han, S. J.; He, Q.; Balke, N.; Yang, C. H.; Lee, D.; Hu, W.; Zhan, Q.; Yang, P. L.; Fraile-Rodriguez, A.; Scholl, A.; Wang, S. X.; Ramesh, R. *Nat. Mater.* **2008**, *7*, 478−482.

(3) Ramesh, R.; Spaldin, N. A. *Nat. Mater.* **2007**, *6*, 21−29.

(4) Han, J.; Hu, J.; Wang, S. X.; He, J. *J. Appl. Phys.* **2015**, *117*, 17A304.

(5) Ryu, J.; Kang, J.-E.; Zhou, Y.; Choi, S.-Y.; Yoon, W.-H.; Park, D.-S.; Choi, J.-J.; Hahn, B.-D.; Ahn, C.-W.; Kim, J.-W.; Kim, Y.-D.; Priya, S.; Lee, S. Y.; Jeong, S.; Jeong, D.-Y. *Energy Environ. Sci.* **2015**, *8*, 2402−2408.

(6) Liu, G.; Ci, P.; Dong, S. *Appl. Phys. Lett.* **2014**, *104*, 032908.

(7) Han, J.; Hu, J.; Wang, S. X.; He, J. *Appl. Phys. Lett.* **2014**, *104*, 093901.

(8) Qiu, J.; Chen, H.; Wen, Y.; Li, P.; Yang, J.; Li, W. *J. Appl. Phys.* **2014**, *115*, 17E522.

(9) Patil, D. R.; Zhou, Y.; Kang, J.-E.; Sharpes, N.; Jeong, D.-Y.; Kim, Y.-D.; Kim, K. H.; Priya, S.; Ryu, J. *APL Mater.* **2014**, *2*, 046102.

(10) Zhang, C. L.; Chen, W. Q. *Appl. Phys. Lett.* **2010**, *96*, 123507.

DOI: 10.1021/acs.nanolett.7b05248
Nano Lett. 2018, 18, 2835−2843

(11) Zhang, C. L.; Yang, J. S.; Chen, W. Q. *Appl. Phys. Lett.* **2009**, *95*, 013511.
(12) Dong, S.; Zhai, J.; Li, J.; Viehland, D. *Appl. Phys. Lett.* **2006**, *88*, 082907.
(13) Dong, S.; Zhai, J.; Bai, F.; Li, J.-F.; Viehland, D. *Appl. Phys. Lett.* **2005**, *87*, 062502.
(14) Chen, F.; Wang, X.; Nie, Y.; Li, Q.; Ouyang, J.; Feng, Z.; Chen, Y.; Harris, V. G. *Sci. Rep.* **2016**, *6*, 28206.
(15) Ciomaga, C. E.; Avadanei, O. G; Dumitru, I.; Airimioaei, M.; Tascu, S.; Tufescu, F.; Mitoseriu, L. *J. Phys. D: Appl. Phys.* **2016**, *49*, 125002.
(16) Wei, Y.; Gao, C.; Chen, Z.; Xi, S.; Shao, W.; Zhang, P.; Chen, G.; Li, J. *Sci. Rep.* **2016**, *6*, 30002.
(17) Mandal, P.; Pitcher, M. J.; Alaria, J.; Niu, H.; Zanella, M.; Claridge, J. B.; Rosseinsky, M. J. *Adv. Funct. Mater.* **2016**, *26*, 2523−2531.
(18) Barman, R.; Kaur, D. *Appl. Phys. Lett.* **2016**, *108*, 092404.
(19) Scott, J. F. *Nat. Mater.* **2007**, *6*, 256−257.
(20) Chu, Y.-H.; Martin, L. W.; Holcomb, M. B.; Gajek, M.; Han, S.-J.; He, Q.; Balke, N.; Yang, C.-H.; Lee, D.; Hu, W.; Zhan, Q.; Yang, P.-L.; Fraile-Rodriguez, A.; Scholl, A.; Wang, S. X.; Ramesh, R. *Nat. Mater.* **2008**, *7*, 478−482.
(21) Jayakumar, O. D.; Mandal, B. P.; Majeed, J.; Lawes, G.; Naik, R.; Tyagi, A. K. *J. Mater. Chem. C* **2013**, *1*, 3710−3715.
(22) Liu, G.; Dong, S. *J. Appl. Phys.* **2014**, *115*, 084112.
(23) Tang, Z. H.; Tang, M. H.; Lv, X. S.; Cai, H. Q.; Xiao, Y. G.; Cheng, C. P.; Zhou, Y. C.; He, J. *J. Appl. Phys.* **2013**, *113*, 164106.
(24) Fina, I.; Dix, N.; Rebled, J. M.; Gemeiner, P.; Marti, X.; Peiro, F.; Dkhil, B.; Sanchez, F.; Fabrega, L.; Fontcuberta, J. *Nanoscale* **2013**, *5*, 8037−8044.
(25) Li, T. X.; Wang, H. W.; Ju, L.; Tang, Z. J.; Ma, D. W.; Li, K. S. *Phys. B* **2015**, *475*, 32−34.
(26) Tingxian, L.; Kuoshe, L. *J. Appl. Phys.* **2014**, *115*, 044316.
(27) Lazenka, V.; Lorenz, M.; Modarresi, H.; Bisht, M.; Ruffer, R.; Bonholzer, M.; Grundmann, M.; Van Bael, M. J.; Vantomme, A.; Temst, K. *Appl. Phys. Lett.* **2015**, *106*, 082904.
(28) Chaudhuri, A. R.; Krupanidhi, S. B.; Mandal, P.; Sundaresan, A. *J. Appl. Phys.* **2009**, *106*, 054103.
(29) Ma, Y. G.; Cheng, W. N.; Ning, M.; Ong, C. K. *Appl. Phys. Lett.* **2007**, *90*, 152911.
(30) Meyer, T. L.; Herklotz, A.; Lauter, V.; Freeland, J. W.; Nichols, J.; Guo, E. J.; Lee, S.; Ward, T. Z.; Balke, N.; Kalinin, S. V.; Fitzsimmons, M. R.; Lee, H. N. *Phys. Rev. B: Condens. Matter Mater. Phys.* **2016**, *94*, 174432.
(31) Ma, X.; Kumar, A.; Dussan, S.; Zhai, H.; Fang, F.; Zhao, H. B.; Scott, J. F.; Katiyar, R. S.; Lupke, G. *Appl. Phys. Lett.* **2014**, *104*, 132905.
(32) Leufke, P. M.; Kruk, R.; Brand, R. A.; Hahn, H. *Phys. Rev. B: Condens. Matter Mater. Phys.* **2013**, *87*, 094416.
(33) Lu, H.; George, T. A.; Wang, Y.; Ketsman, I.; Burton, J. D.; Bark, C. W.; Ryu, S.; Kim, D. J.; Wang, J.; Binek, C.; Dowben, P. A.; Sokolov, A.; Eom, C. B.; Tsymbal, E. Y.; Gruverman, A. *Appl. Phys. Lett.* **2012**, *100*, 232904.
(34) Vaz, C. A. F.; Segal, Y.; Hoffman, J.; Grober, R. D.; Walker, F. J.; Ahn, C. H. *Appl. Phys. Lett.* **2010**, *97*, 042506.
(35) Vaz, C. A. F.; Hoffman, J.; Segal, Y.; Reiner, J. W.; Grober, R. D.; Zhang, Z.; Ahn, C. H.; Walker, F. J. *Phys. Rev. Lett.* **2010**, *104*, 127202.
(36) Molegraaf, H. J. A.; Hoffman, J.; Vaz, C. A. F.; Gariglio, S.; van der Marel, D.; Ahn, C. H.; Triscone, J. M. *Adv. Mater.* **2009**, *21*, 3470−3474.
(37) Burton, J. D.; Tsymbal, E. Y. *Phys. Rev. B: Condens. Matter Mater. Phys.* **2009**, *80*, 174406.
(38) Zhao, Y. Y.; Wang, J.; Hu, F. X.; Liu, Y.; Kuang, H.; Wu, R. R.; Sun, J. R.; Shen, B. G. *AIP Adv.* **2016**, *6*, 055814.
(39) Zhao, Y. Y.; Wang, J.; Kuang, H.; Hu, F. X.; Liu, Y.; Wu, R. R.; Zhang, X. X.; Sun, J. R.; Shen, B. G. *Sci. Rep.* **2015**, *5*, 9668.
(40) Zheng, R. K.; Wang, Y.; Liu, Y. K.; Gao, G. Y.; Fei, L. F.; Jiang, Y.; Chan, H. L. W.; Li, X. M.; Luo, H. S.; Li, X. G. *Mater. Chem. Phys.* **2012**, *133*, 42−46.
(41) Thiele, C.; Dorr, K.; Bilani, O.; Rodel, J.; Schultz, L. *Phys. Rev. B: Condens. Matter Mater. Phys.* **2007**, *75*, 054408.
(42) Eerenstein, W.; Wiora, M.; Prieto, J. L.; Scott, J. F.; Mathur, N. D. *Nat. Mater.* **2007**, *6*, 348−351.
(43) Kim, J. Y.; Yao, L.; van Dijken, S. *J. Phys.: Condens. Matter* **2013**, *25*, 082205.
(44) Martin, M. C.; Shirane, G.; Endoh, Y.; Hirota, K.; Moritomo, Y.; Tokura, Y. *Phys. Rev. B: Condens. Matter Mater. Phys.* **1996**, *53*, 14285−14290.
(45) Janotti, A.; Jalan, B.; Stemmer, S.; Van de Walle, C. G. *Appl. Phys. Lett.* **2012**, *100*, 262104.
(46) Noheda, B.; Gonzalo, J. A.; Cross, L. E.; Guo, R.; Park, S. E.; Cox, D. E.; Shirane, G. *Phys. Rev. B: Condens. Matter Mater. Phys.* **2000**, *61*, 8687−8695.
(47) Guo, E. J.; Roth, R.; Herklotz, A.; Hesse, D.; Dorr, K. *Adv. Mater.* **2015**, *27*, 1615−1618.
(48) Haun, M. J.; Furman, E.; Jang, S. J.; Cross, L. E. *Ferroelectrics* **1989**, *99*, 63−86.
(49) Vrejoiu, I.; Le Rhun, G.; Pintilie, L.; Hesse, D.; Alexe, M.; Gösele, U. *Adv. Mater.* **2006**, *18*, 1657−1661.
(50) Yang, F.; Kemik, N.; Biegalski, M. D.; Christen, H. M.; Arenholz, E.; Takamura, Y. *Appl. Phys. Lett.* **2010**, *97*, 092503.
(51) Catalan, G. *Appl. Phys. Lett.* **2006**, *88*, 102902.
(52) Chandrasekhar, K. D.; Das, A. K.; Mitra, C.; Venimadhav, A. *J. Phys.: Condens. Matter* **2012**, *24*, 495901.
(53) Tang, R. J.; Jiang, C.; Qian, W. H.; Jian, J.; Zhang, X.; Wang, H. Y.; Yang, H. *Sci. Rep.* **2015**, *5*, 13645.
(54) Makosz, J. J.; Urbanowicz, P. *Z. Naturforsch., A: Phys. Sci.* **2002**, *57*, 119−125.
(55) Jonscher, A. K. *Dielectric relaxation in solids*; Chelsea Dielectrics Press: London, 1983; pp 13−380.
(56) Guerra, J. D. S.; Eiras, J. A. *J. Phys.: Condens. Matter* **2007**, *19*, 386217.
(57) Arlt, G.; Pertsev, N. A. *J. Appl. Phys.* **1991**, *70*, 2283−2289.
(58) McNeal, M. P.; Jang, S. J.; Newnham, R. E. *J. Appl. Phys.* **1998**, *83*, 3288−3297.
(59) McGilly, L. J.; Feigl, L.; Sluka, T.; Yudin, P.; Tagantsev, A. K.; Setter, N. *Nano Lett.* **2016**, *16*, 68−73.
(60) McGilly, L. J.; Yudin, P.; Feigl, L.; Tagantsev, A. K.; Setter, N. *Nat. Nanotechnol.* **2015**, *10*, 145−150.
(61) Li, X. W.; Gupta, A.; Xiao, G.; Gong, G. Q. *Appl. Phys. Lett.* **1997**, *71*, 1124−1126.
(62) Liao, J. H.; Wu, T. B. *Electrochem. Solid-State Lett.* **2007**, *10*, P27−P30.
(63) Liao, J. H.; Wu, T. B.; Chen, Y. T.; Wu, J. M. *J. Appl. Phys.* **2007**, *101*, 09M110.
(64) Spurgeon, S. R.; Balachandran, P. V.; Kepaptsoglou, D. M.; Damodaran, A. R.; Karthik, J.; Nejati, S.; Jones, L.; Ambaye, H.; Lauter, V.; Ramasse, Q. M.; Lau, K. K. S.; Martin, L. W.; Rondinelli, J. M.; Taheri, M. L. *Nat. Commun.* **2015**, *6*, 6735.
(65) Li, J.; Lu, Y. J.; Ye, Q.; Cinke, M.; Han, J.; Meyyappan, M. *Nano Lett.* **2003**, *3*, 929−933.
(66) Currie, L. A. *Pure Appl. Chem.* **1995**, *67*, 1699−1723.

DOI: 10.1021/acs.nanolett.7b05248
Nano Lett. 2018, 18, 2835−2843